Dipole-Based Filtering for Improved Removal of Background Field Effects from 3D Phase Data

S. J. Wharton[1], and R. Bowtell[1]
[1]Sir Peter Mansfield Magnetic Resonance Centre, University of Nottingham, Nottingham, United Kingdom

Introduction: Phase images of the brain generated using gradient echo sequences at high field strength show excellent contrast attributed to small field perturbations produced by susceptibility differences between tissues. In order to reveal the small phase variations related to the local anatomy it is however necessary to eliminate the large field offsets caused by remote tissue/air interfaces, such as those that are present in the sinuses. These unwanted field shifts are generally removed by filtering the phase images using a variety of methods, including: (i) Fourier-based filtering where the data is converted into complex form, low-pass filtered, and divided into the original data [1]; (ii) subtraction of a low-order polynomial fit to the data [2]; (iii) subtracting off an estimate of the field perturbation produced by the sinuses based on information from T_1-weighted images [3]. Unfortunately, methods (i) and (ii) tend to remove the desired anatomical structure as well as the unwanted external fields, while method (iii) requires additional image data from which the location of the sinuses can be inferred. Here we present a method for selectively eliminating the externally generated field shifts without the need for additional scans, using one or more dipole point sources situated outside the region of interest (ROI) being considered. The method was tested on simulated and experimentally acquired phase data spanning the red nucleus (RN) and substantia nigra (SN), which show the effect of strong unwanted fields due to the close proximity of the sinuses.

Theory and Methods: Equation [1] shows how the field shift ΔB_z^{dip} at position, $\mathbf{r}$, due to an axially oriented magnetic dipole can be expressed as a function of four parameters representing, the strength, P, and position, $\mathbf{r_d} = x_d\hat{\mathbf{x}} + y_d\hat{\mathbf{y}} + z_d\hat{\mathbf{z}}$, of the dipole.

$$\Delta B_z^{dip}(\mathbf{r}) = \frac{P}{|\mathbf{r}-\mathbf{r_d}|^3}\left(3\left(\frac{(\mathbf{r}-\mathbf{r_d})\hat{\mathbf{z}}}{|\mathbf{r}-\mathbf{r_d}|}\right)^2 - 1\right) \qquad \textbf{Eq.[1]}$$

The first stage in the filtering process is to vary these four parameters, limiting the dipole position to the region outside the ROI, until a minima is reached in the difference between ΔB_z^{dip} and the field map calculated from the phase data, ΔB_z. More dipoles can then be arranged in fixed positions around the original dipole and a least squares fit carried out to identify the dipole strengths that best model ΔB_z, before subtraction of ΔB_z^{dip} from ΔB_z. The performance of the dipole filtering method was evaluated by applying it to simulated data from the SN and RN, comprising a known combination of realistic, internally-generated fields, ΔB_z^{RNSN} (Fig. 2a-c) and externally-generated fields due the frontal sinus, ΔB_z^{EXT} (Fig. 2d). These were generated by applying a forward field calculation [4] to a segmented model of the RN and SN and to the HUGO body model. For comparison, the effects of the polynomial and Fourier-based filters were also evaluated. Two parameters were used to characterise the performance of each filter: a contrast parameter $f_c = F(\Delta B_z^{RNSN}) / \Delta B_z^{RNSN}$, reflecting the reduction of the field from the RN&SN due to filtering and an error parameter $f_e = |F(\Delta B_z^{EXT})|$, reflecting the residual externally generated field after filtering. Here F is the filter function and the ideal values for f_c and f_e are 1 and 0 respectively.

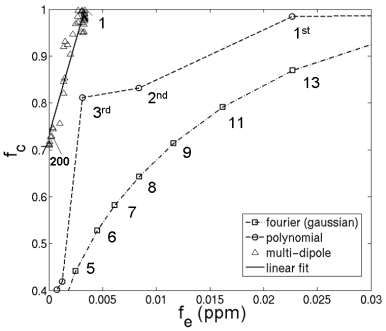

***Figure 1** Plot of f_c vs f_e for each filtering method with data labels indicating filter parameters.*

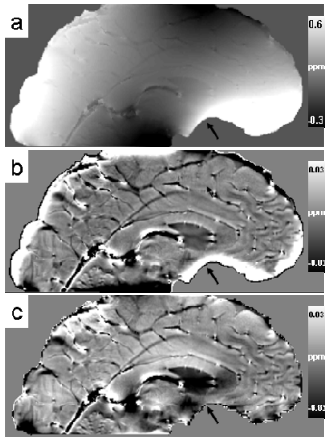

***Figure 3** Sagittal slice of whole head unwrapped phase (a), and filtered phase using Fourier (b) and dipole filters (c), arrows show location of sinuses.*

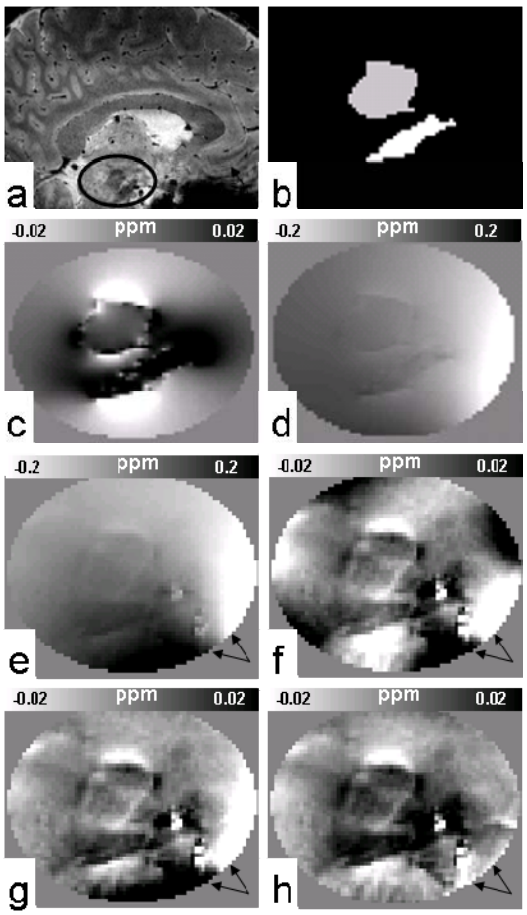

***Figure 2** Sagittal slice of modulus data (a) used to create RN/SN model (b) (RN = grey, SN = white), the simulated field ΔB_z^{RNSN} due to b (c), plus simulated sinus field ΔB_z^{EXT} (d). In-vivo phase data spanning RN/SN (e), filtered using polynomial (f), Fourier (g), and dipole (h) filters.*

Results: Fig. 1 shows plots of f_c versus f_e for each of the three filters on varying the characteristic filter parameter: the FWHM in mm of the Gaussian filter used in the Fourier method, the maximum order of the 3D polynomial used in the polynomial filter, and the number of dipoles used in the dipole filter. The optimum values for each of the filtering methods were then chosen (FWHM = 6mm, 3rd order polynomial, and 10 dipoles) and applied to in-vivo phase data (Fig 2e) acquired at 7T on a Philips Achieva scanner using a standard FLASH sequence, TE/TR = 20/50ms, isotropic 0.5mm resolution , spanning the region of the RN/SN, see Figs. 2f-h. The Fourier and dipole filters were also applied to whole head phase data (Fig. 3), in this case the dipole filter was combined with subtraction of a 2nd order polynomial fit to the data which accounted for large length-scale field variations due to imperfect shim settings.

Discussion: The plot of f_c vs f_e (Fig.1) shows that the dipole filter outperforms the Fourier and polynomial methods in preserving contrast and removing the externally generated unwanted fields in the simulated data. In agreement with the simulations, the dipole filter also performed excellently in removing the rapidly varying sinus fields towards the edge of the ROI in the *in vivo* data while the other methods left considerable residual field (see arrows in Fig.2 f-h). The whole head results obtained by using the dipole filter combined with a 2nd order polynomial, shown in Fig3, show a clear reduction of edge artefacts close to the sinuses when compared with results obtained by using the Fourier-based filter. The results presented here suggest that dipole based high-pass filtering has the potential to be an important tool in the processing of phase data for SWI and susceptibility mapping. Further work is being carried out to optimise this new filtering method for in-vivo applications.

References:[1] Haacke et al. 2005.MRI. 23:1-25.[2] Duyn et al. 2007. PNAS 104:11796-11801.[3] Neelavalli et al. 2009. JMRI. 29.937. [4] Schaefer et al. Neuroimage. 2009. 48:126-137.